ORIGINAL PAPER

DEER/PELDOR Study of the Effect of Extremely Low Concentrations of the Antimicrobial Peptide Chalciporin A on the Membrane Lipid Organization

Anna S. Kashnik[1] · Victoria N. Syryamina[1] · Barbara Biondi[2,3] · Cristina Peggion[2,3] · Fernando Formaggio[2,3] · Sergei A. Dzuba[1,4]

© The Author(s), under exclusive licence to Springer-Verlag GmbH Austria, part of Springer Nature 2023

Abstract

Antimicrobial peptides (AMPs) are promising therapeutic agents against drug-resistant bacteria. Many AMPs can directly interact with bacterial membranes, disturbing their integrity and/or functionality. Chalciporin A is a naturally occurring 14-mer AMP, belonging to the class of peptaibiotic. Spin-label electron paramagnetic resonance in its pulsed versions is a suitable tool to study intermolecular interactions in biological media. Here, we applied double electron–electron resonance (DEER, also known as PELDOR) and electron spin echo envelope modulation, to study model membranes of palmitoyl-oleoyl-glycero-phosphocholine in the presence of chalciporin A. The spin-labeled molecules were either chalciporin A or doxyl-spin-labeled stearic acids (DSAs). We observed that chalciporin A influences DSA clustering, disturbing the formation of the alternative sub-clusters in two opposing leaflets that was recently found in peptide-free membranes (Smorygina et al. in Langmuir 37:13909–13916, 2021). The intriguing point of this influence is that it takes place for peptide concentrations as small as 0.01 mol% (1/10,000 peptide-to-lipid ratio). The possible reasons for this membrane perturbation at extremely low concentrations are discussed.

✉ Sergei A. Dzuba
  dzuba@kinetics.nsc.ru

[1] Voevodsky Institute of Chemical Kinetics and Combustion, RAS, Novosibirsk 630090, Russian Federation

[2] Padova Unit, Institute of Biomolecular Chemistry, CNR, 35131 Padua, Italy

[3] Department of Chemical Sciences, University of Padova, 35131 Padua, Italy

[4] Department of Physics, Novosibirsk State University, 630090 Novosibirsk, Russian Federation

1 Introduction

As the spreading of antibiotic-resistance bacteria increases the risk of serious infections and threatens public health, it is important to search for new antibacterial drugs, able to overcome bacterial resistance [1–4]. Antimicrobial peptides (AMP) are promising candidates due to their high metabolic activity, high rate of bactericidal action, low likelihood of addiction and side effects [4, 5].

AMPs are isolated from natural agents (fungi, insects or vertebrates) [6] as a mixture of analogs with different affinity and activity against pathogens [7]. With the help of drug design, it is possible to strongly modify the physicochemical properties of AMPs to increase their enzymatic stability, to decrease their cytotoxicity, or to enhance selectivity and activity against pathogens [8–13].

Among the variety of AMPs, a standing out subclass is represented by the membrane-active peptides (MAPs), which act by binding the phospholipid membrane and altering its structure [14]. Since the peptide-membrane interaction is driven by hydrophobic and electrostatic forces, resistance to MAPs action is hardly expected [6]. The peptide-induced changes to the lipid membrane cause stress in the local membrane curvature [15], alteration of the lipid lateral mobility or lipid chain ordering [16–19], formation or disruption of local domains [19–23], or formation of conductive channels or pores [24–26]. As a result, the local mechanical properties or transport function of the membrane are altered, the membrane becomes more vulnerable, and cell lysis occurs via pore formation or membrane disruption [27].

In addition to the pore-formation mechanism of the MAP antimicrobial action, also other membrane disruption mechanisms were proposed. Small-angle neutron scattering (SANS) data [22] demonstrated that a low concentration of peptide alamethicin (0.5 mol%) disrupts a lateral inhomogeneity in cholesterol-containing lipid vesicles [22]. It was shown that peptide aurein induces lateral segregation of lipids without forming pores or destroying membranes [19]. Pulsed electron paramagnetic resonance (EPR) of spin-labeled free fatty acids showed that these molecules are assembled around the peptide molecules of alameticin [28] and trichogin [29].

Here, we study at the molecular level the mechanism of action of the membrane-active peptide chaciporin A. This peptide belongs to the subclass of medium-length peptaibols (from 14- to 16-mers) and is close to the family of tylopeptins, also isolated from the fruitful body of *Sepedonium chalcipori*. It is active both against Gram-positive and Gram-negative bacteria [30]. As the activity of MAPs is known to correlate with their ability to cause the lateral reorganization of charged lipids or lipid-like molecules [18, 20–22, 31, 32], up to the formation of conductive pores [25], we study here the influence of chalciporin A on the nanoscale clusters formed by guest-free fatty acids (FFAs).

Fatty acids and their derivatives are abundant in biological membranes, mainly as components of phospholipids and cholesterol esters; their presence is known to affect the structural properties of membranes [33]. Also, FFAs have an important role in lipid metabolism [34], regulate the membrane fluidity, and have a

protective function. Their numbers increase under certain pathological conditions in the cell [35]. In addition, FFAs may serve as a relevant model of bacterial membranes which are known to contain a significant portion of anionic lipids [36, 37]. The phenomenon of FFA clustering in model membranes has been recently discovered by pulse EPR techniques [28, 29, 38]. It is reasonable to assume that the peptide-induced reorganization of these clusters might determine the peptide activity [20].

To examine how chalciporin A induces changes on the lateral lipid organization, we exploited the spin-labeled analogs of FFA, 5- and 16-doxyl stearic acids (5-DSA and 16-DSA, respectively) in zwitter-ionic phospholipid membranes of 1-palmitoyl-2-oleoyl-*sn*-glycero-3-phosphocholine (POPC). These species were studied by EPR techniques, in its both conventional continuous wave (CW) and pulse versions. Note that although the pulsed EPR is applied mainly for solids, the results obtained at low temperature may provide a clue for understanding processes at physiological temperatures. Pulsed EPR is based on the electron spin echo (ESE) phenomenon. Two versions of ESE experiments were employed: double electron–electron resonance (DEER, also known as PELDOR) [39–43] which probes molecular self-assembling, and electron spin echo envelope modulation (ESEEM) [44–47], which probes the peptide localization in the membrane.

2 Experimental

2.1 Materials

The sequences of chalciporin A (Chalc) and its spin-labeled analog (Chalc-SL) are given in Table 1 (see also Fig. S1 in Supplementary Information). These peptides were synthesized by solid-phase, following published procedures [30].

Here, Ac is the acetyl, Lol is the 1,2-amino alcohol leucinol, Aib is α-aminoisobutyric acid, and TOAC is 2,2,6,6-tetramethylpiperidine-1-oxyl-4-amino-4-carboxylic acid (spin label).

Lipids POPC were from Avanti Polar Lipids (Birmingham, AL, USA). Spin-labeled stearic acids 5-DSA and 16-DSA were from Sigma-Aldrich (Saint Louis, MO, USA). Chemical structures of POPC, 5-DSA and 16-DSA are shown in Fig. S1. All compounds were used without further purification.

2.2 Sample Preparation

Two types of samples were prepared. First, POPC bilayers were mixed with 0.2 to 2 mol% Chalc-SL. Second, POPC bilayers containing 5- or 16-DSA were mixed with

Table 1 Amino acid sequences and abbreviations for the peptides investigated in this study

Chalc	Ac-Trp-Val-Aib-Val-Ala-Gln-Ala-Aib-Ser-Leu-Ala-Leu-Aib-Gln-Lol
Chalc-SL	Ac-Trp-Ala-Aib-Val-Ala-Gln-Ala-Aib-Ser-Leu-Ala-Leu-**TOAC**-Gln-Lol

0–2 mol% Chalc. All substances were separately dissolved in chloroform, and the solutions then were mixed. Chloroform was removed by a nitrogen stream, and the mixture was stored under vacuum for 4 h. Then, phosphate-buffered saline (contains 0.137 M NaCl and 0.0027 M KCl, pH 7.0) was added in a proportion of 10:1 to hydrate the resulting powder, and this mixture was stored for 2 h at room temperature and stirred occasionally. In some cases, hydration was performed using heavy water ^2H_2O. Upon this procedure, multilamellar vesicles (MLV) are known to be formed [48]. The mixture then was centrifuged to remove the excess water. The prepared samples were put into EPR glass tubes of 3 mm o.d. which were then quickly frozen by immersion into liquid nitrogen.

2.3 Measurements

Continuous wave (CW) EPR spectra at room temperature were obtained with an X-band EPR benchtop SPINSCAN-X spectrometer (ADANI, Minsk, Belarus). The modulation amplitude was 0.01 mT, the output microwave (MW) power was 100 mW, the MW attenuation was -25 dB, the sweep and constant times were of 60 s and 46 ms, respectively. CW EPR spectra at reduced temperature (200 K) were obtained with an X-band Bruker ELEXSYS E580 EPR spectrometer using a Bruker ER 4118X-MD5 dielectric resonator, which was placed in an Oxford Instruments CF 935 cryostat. The modulation amplitude was 0.01 mT, the output MW power was 200 mW, the MW attenuation was -25 dB, the sweep and constant times were of 10.49 s and 20.48 ms, respectively.

In pulsed EPR studies, the X-band Bruker ELEXSYS E580 EPR spectrometer was used, equipped with a split-ring Bruker ER 4118 X-MS-3 resonator and an Oxford Instruments CF-935 cryostat. A three-pulse DEER measuring scheme [39, 40, 43] was employed, $(\pi/2)_{\nu A}$-t-$\pi_{\nu B}$-$(t-\tau)$-$\pi_{\nu A}$-τ-$echo_{\nu A}$, where the subscripts stand for MW frequency. The lengths of the first and second pulses applied at the frequency ν_A were 16 and 32 ns, respectively, the pumping pulse applied at the frequency ν_B was of 36 ns length, and its amplitude was adjusted to provide a π turning angle via nutation experiment. The time delay τ was 350 and 500 ns in the case of experiments with the Chalc-SL, and 700 ns in the case of the DSAs. The pumping pulse delay t was scanned with a step of 4 ns, starting at $t = -200$ ns (i.e., prior to the first detection pulse). The frequency ν_B in the applied spectrometer magnetic field B_0 corresponded to excitation of the maximum of the echo-detected EPR spectrum. The difference $\nu_A - \nu_B$ between the detection and pumping frequencies was 70 MHz for the samples of the first kind (see above) and -85 MHz for the samples of the second kind—see Fig. S2. The DEER signal distortion upon the pumping pulse passage through the detecting pulses was corrected by comparison with the "blank" excitation experiment, as described previously [49], and some details are given in Fig. S3.

The samples hydrated with heavy water were studied using ESEEM experiments, in which the three-pulse sequence $(\pi/2)$-τ-$(\pi/2)$-t-$(\pi/2)$-τ-$echo$ (of the same MW frequency) was employed, with excitation at the maximum of the echo-detected EPR

spectrum. The pulse lengths were 16 ns, the time delay τ was 204 ns, and the time delay t was scanned from 300 ns to 8.5 μs, with a 12 or 16 ns time step.

In the DEER and ESEEM measurements, the sample temperature was kept near 80 K. In all measurements at the reduced temperature, the resonator was cooled with a stream of cold nitrogen gas. The temperature was stabilized by a Bruker ER4131VT temperature controller.

3 Results

3.1 CW EPR and DEER of Chalc-SL: Interaction with the Membrane and Lateral Distribution

CW EPR of Chalc-SL in POPC bilayers taken at room temperature did not differ from analogous data previously reported [30]. These spectra are typical for the membrane-bound peptides (see e.g., [50, 51]), evidencing that the Chalc-SL molecules are bound to the membrane.

Figure 1 shows the CW EPR spectra of Chalc-SL taken at low temperature (200 K) at two different concentrations. These spectra are also typical for immobilized nitroxides—see e.g., [51–53]. These spectra do not possess an additional line broadening, even at the largest Chalc-SL concentration studied (2 mol%), which one may expect to appear because of magnetic dipole–dipolar interaction between electron spins occurring upon aggregation of spin labels [51–53]. The detailed simulations [52] showed that dipolar broadening becomes inessential for spin labels separated by the distances larger than 1.5 nm. Therefore, we may conclude that Chalc-SL (and Chalc) molecules are not prone to aggregation.

DEER spectroscopy allows studying magnetic dipole–dipolar interactions between unpaired electron spins of spin-labeled molecules, in the larger distance scale of several nanometers. For random distribution of spin labels in a three-dimensional space, the DEER signal decays exponentially [40, 41]:

Fig. 1 CW EPR spectra at 200 K for Chalc-SL at two concentrations in the POPC bilayer. The data are shifted upward for convenience
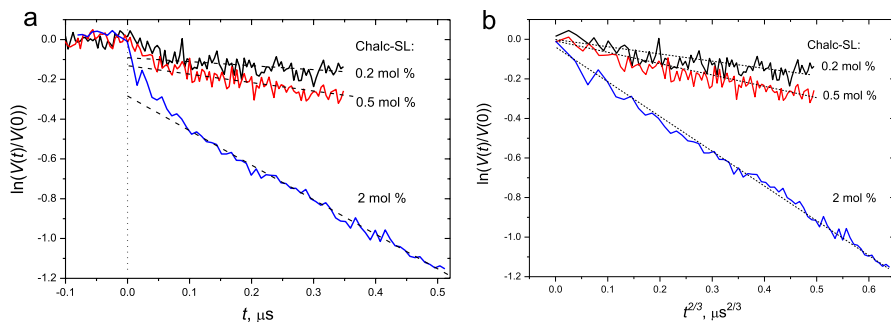
Chalc-SL:

0.5 mol %

2 mol %
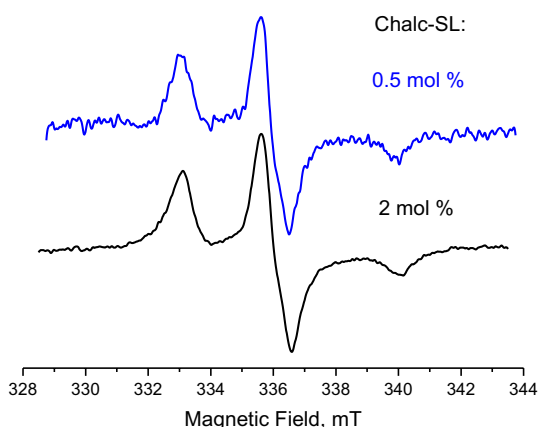
Fig. 2 Semilogarithmic plot for the three-pulse DEER time traces for Chalc-SL at three different concentrations of spin-labeled peptide Chalc-SL. **a** Data are plotted as a function of t, with dashed straight lines showing linear asymptotic; **b** data are plotted as a function of $t^{2/3}$, with dashed lines showing linear approximations

$$V_{3D}(t) = \exp\left(-\frac{8\pi^2}{9\sqrt{3}} \frac{g^2 \mu_B^2}{\hbar} C_{local} p_B t \right), \tag{1}$$

where g is the g-factor, μ_B is the Bohr magneton, C_{local} is the local concentration in cm^{-3} units, and the dimensionless parameter p_B determines the efficiency of pulse excitation of the EPR spectrum. For the experimental conditions of this work, p_B is expected to be close to 0.2 [54]. The concept of local concentrations appears in the case of heterogeneous spin-label distribution; for the case of homogeneous distribution C_{local} coincides with the total concentration C.

Note that Eq. (1) may be used for clusters of spin labels containing randomly distributed spins with their number N large enough to consider these clusters as infinite. From the detailed simulations [53], it can be concluded that this takes place for N larger than ∼ 100.

For biological membranes, two-dimensional distribution of spin labels may become more appropriate. In this case, instead of exponential behavior described by Eq. (1), the dependence of the form $V(t) = \exp(-\text{const } \sigma_{local} p_B t^{2/3})$ takes place [40], where σ_{local} is the local surface concentration. Numerical simulations [55] have shown that in this case:

$$V_{2D}(T) \cong \exp\left(-3.37 \sigma_{local} p_B (g^2 \mu_B^2 t / \hbar)^{\frac{2}{3}} \right), \tag{2}$$

where σ_{local} is taken in cm^{-2} units. For the case of homogeneous distribution, σ_{local} coincides with the total concentration σ, and when spin labels are arranged into oligomers with the inter-spin distance of several nanometers, the DEER signal experiences fast initial decay substituted then by the asymptotic dependences given by Eqs. (1) or (2) [40–42].

Figure 2 presents semilogarithmic plot of DEER time traces obtained for Chalc-SL at three different concentrations in the POPC bilayers. Data are given in two variants—with the abscissa taken as t (Fig. 2a) and as $t^{2/3}$ (Fig. 2b)—to compare

with Eqs. (1) and (2), correspondingly. One can see that in Fig. 2a, the DEER signal experiences fast initial decay (when $t < 0.1$ μs) that is then substituted by a linear decay; in Fig. 2b the all-time traces are linear.

These two data presentations allow two alternative explanations. Data in Fig. 2a may be interpreted as an evidence that Chalc-SL molecules are assembled in oligomers (fast decay at the beginning), with random three-dimensional space distribution of oligomers (exponential asymptotic decay). Data of Fig. 2b may be interpreted within a simpler model that Chalc-SL molecules are randomly distributed in two-dimensional space. These two possibilities can be discriminated by quantitative comparing with theoretical Eqs. (1) and (2). Using $p_B = 0.2$ (see above) and the volume concentration of the lipids in the bilayer assessed as $C_{lipids} \sim 8 \times 10^{20}$ cm^{-3} (that can be assessed from data in [56]), one obtains from Eq. (1) that the local Chalc-SL concentration C_{local} is about three times less than the mean concentrations C in the membrane, in all three cases of the 0.2, 0.5 and 2 mol% samples. This decrease could be due to partial loss of spin labels during storage, but in this study we used freshly prepared samples, so this possibility can be ruled out. Meanwhile, using the surface lipid concentration of $\sim 1.7\ 10^{14}$ cm^{-2}, estimated from the known area per lipid [57] (0.6 nm^2), it can be reasonably estimated for σ_{local} that it is close to the mean surface concentration σ. So, we conclude that most probably the spin labels are randomly distributed in two-dimensional space, which also means that Chalc-SL molecules are not prone to oligomerization.

3.2 ESEEM of Chalc-SL: Peptide Localization in the Bilayer

ESE envelope modulation (ESEEM) appears because of interaction between unpaired electron of a spin label and the nearby nuclei. To select the nuclei of interest, deuteration is employed. For D$_2$O-hydrated bilayers, the ^{2}H-ESEEM signal gives information about the local water concentration, at distances in the range of 0.1–1 nm from the unpaired electron of the spin label [44–47]; these data provide information on the spin probe immersion depth across the bilayer.

Here, we studied ^{2}H-ESEEM in the Chalc-SL/POPC D$_2$O-hydrated bilayers. The obtained ESEEM time trace, as a function of the delay t between the second and the third pulses, $E(t)$ (see "Experimental") was refined from the influence of the non-modulated spin relaxation by normalizing to the mean echo decay [44–47]:

$$E_n(t) = \frac{E(t)}{< E(t) >} - 1, \tag{3}$$

where $< E(t) >$ is a non-oscillating smooth function approximating the original average $E(t)$ time trace. The result is shown in Fig. 3a, along with the analogously obtained reference data on spin-labeled stearic acids, 5- 12- and 16-DSA [58] and on 2-oleoyl-1-palmitoyl-sn-glycero-3-phospho(tempo)choline (denoted here as TEMPO-PC) [59]. In the latter case, the spin label is attached to the polar lipid head, thus being exposed to the water shell hydrating the bilayer.

The ESEEM signal treatment by Eq. (3) allows quantifying the strength of electron-nuclear interaction for the remote nuclei, by comparing the modulation
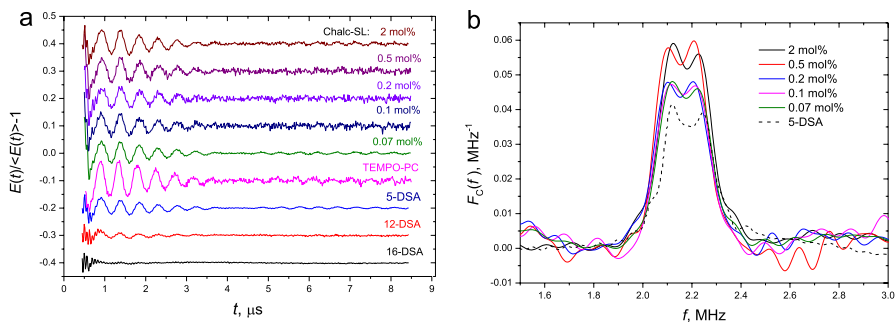
Fig. 3 **a** ESEEM time traces for Chalc-SL at different concentrations (indicated) in the D_2O-hydrated POPC bilayer. For comparison, the analogous data for 5-, 12-, 16-DSA and TEMPO-PC are given (see text). The data are vertically shifted for convenience. **b** Cosine Fourier transforms of ESEEM time traces for Chalc-SL at different concentrations (solid lines) and for 5-DSA (dashed line)

amplitudes for different samples. It can be seen from Fig. 3a that, first, these amplitudes for Chalc-SL are smaller than for TEMPO-PC, are significantly larger than for 12- and 16-DSA, and are close to those for 5-DSA. Since the spin label in TEMPO-PC is in direct contact with hydrating water, in 12- and 16-DSA it is located in the membrane interior, and in 5-DSA it is located between these two extreme positions, it can be stated that the Chalc-SL spin label is also embedded between these two extreme positions in the membrane. Secondly, Fig. 3a shows that the modulation amplitudes for Chalc-SL are approximately the same for different concentrations.

A more precise comparison of ESEEM amplitudes can be achieved by using Fourier transforms of the time traces in Fig. 2a. These data were obtained according to the approach described in [46]. The results are shown in Fig. 3b. One can see that the approximate closeness seen in the time domain (Fig. 3a) here becomes more quantified. For the two highest concentrations, 0.5 and 2 mol.%, the ESEEM amplitude is slightly larger than for lower concentrations, which means that the spin label is located slightly closer to the membrane surface. The ESEEM amplitudes for Chalc-SL are somewhat larger than those for 5-DSA, which implies that the spin label in Chalc-SL is located a bit closer to the membrane surface than that in 5-DSA.

3.3 DEER of 5(16)-DSAs: The Chalciporin A Impact on Membrane Organization

The CW EPR spectra of 5-DSA and 16-DSA in POPC bilayers—see Figs. S4 and S5—were similar to those previously published [38]. Note that for the 5(16)-DSA concentration above 2 mol%, the CW EPR spectra [38] show additional broadening because of dipole–dipolar interaction, which may imply partial oligomerization and in turn does not allow correct use of DEER technique (which is restricted to distances only above 1.5 nm [40–43]).

In Fig. 4, some representative DEER time traces are shown for 5-DSA and 16-DSA in the POPC bilayer in the presence of Chalc of different concentrations (the full set of DEER time traces is presented in Figs. S6–S9). One can see that in all cases, the data in Fig. 4 approximately obey the exponential behavior predicted
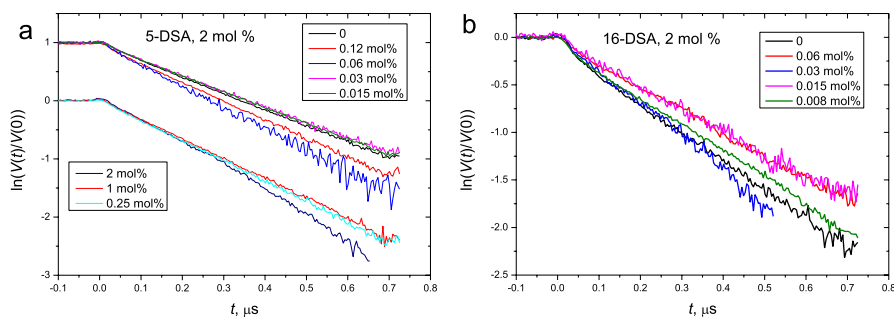
Fig. 4 Representative data for three-pulse DEER time traces for 2 mol% 5-DSA (**a**) and 2 mol% 16-DSA (**b**) in the POPC bilayer at different Chalc concentrations indicated in rectangles

by Eq. (1). This may imply that the spatial positions of steric acids across the membrane are more or less distributed, making the overall distribution closer to the three-dimensional one.

From the slopes of the dependences in Fig. 4 and Figs. S6–S9 using Eq. (1), one can obtain the local volume concentrations of 5(16)-DSA molecules. The p_B values for 5-DSA and 16-DSA were found previously [38] in calibration experiments in ethanol/methanol glass (see also Fig. S10); these values were obtained from the slopes of experimental DEER time traces and turned out to be 0.068 ± 0.001 for 5-DSA and 0.049 ± 0.001 for 16-DSA. Note that the relative smallness of the obtained p_B values reflects partial loss of spin labels upon storage (as compared with $p_B \approx 0.2$ for freshly prepared samples under the same experimental conditions—see above); we believe that this loss under the experimental approach used does not influence our conclusions.

Figure 5 presents the C_{local} values found for 5(16)-DSA in this way in the absence on Chalc, as a function of their mole fraction χ. The data in Fig. 5 are given in dimensionless units, by dividingthe volume concentration of the lipids in the bilayer, C_{lipids} (assessed as $\sim 8 \times 10^{20}$ cm^{-3}, see above). The experimental uncertainty in Fig. 5 was evaluated from the uncertainty of the tangent determination for DEER time traces (see Fig. 4), taking also into account the uncertainty of p_B determination.

One can see in Fig. 5, firstly, that the local concentrations C_{local} for both 5-DSA and 16-DSA exceed χ. This unambiguously implies cluster formation. Secondly, C_{local} is twice as large as χ. This fact may be explained within a "chess box" model for the DSA distribution between two leaflets of the bilayer, which is shown as insert to Fig. 5. Meanwhile, for $\chi = 2$ mol% the C_{local} value for 16-DSA in Fig. 5 becomes larger than that for 5-DSA (this effect was found previously [38]; however, because of annoying arithmetical error, the data [38] for 16-DSA were presented incorrectly).

Figure 6 presents C_{local} values for 5- and 16-DSA obtained as a function of dissolved Chalc, for two 5(16)-DSA concentrations, 1 and 2 mol%. One can see that for 5(16)-DSA concentration of 2 mol% the C_{local} for 16-DSA value at P/L = 0 (i.e. in absence of Chalc) is one and a half times larger than C_{local} for 5-DSA—that corresponds to the data of Fig. 5,—while with the P/L increase these two concentrations tend to become equal. Amazingly, this equalization effect starts at extremely low
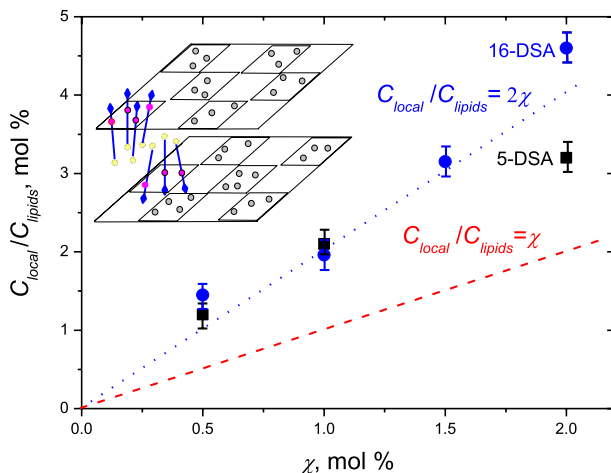
Fig. 5 The local volume concentrations, C_{local} for 16-DSA (circles) and 5-DSA (squares), as a function of their molar content χ. The data were obtained from DEER time traces like those shown in Fig. 4, and are given in dimensionless units, C_{local}/C_{lipids}, where $C_{lipids} = 8 \times 10^{20}$ cm^{-3} (see text). The dashed and dotted lines correspond to the two linear functions indicated in the figure. The insert illustrates a "chess box" model for the DSA distribution between two leaflets of the bilayer, explaining the twofold increase of C_{local}/C_{lipids} value over the χ value
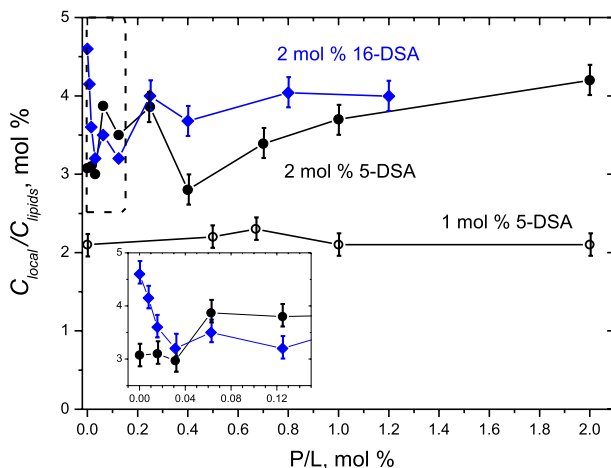
Fig. 6 Local volume concentrations of spin-labeled stearic acids in dimensionless units, C_{local}/C_{lipids}, for 5-DSA and 16-DSA in the POPC membrane as a function of the peptide-to-lipid (P/L) ratio. The data are obtained using Eq. (1) from the DEER time traces like those shown in Fig. 4. The inset shows an enlarged portion of the graph, indicated by a dashed rectangle

peptide concentration, seen already at 0.01 mol% (P/L = 1/10,000). Meanwhile, for 5-DSA concentration of 1 mol% the local concentration does not change with P/L varying—which corresponds to their similar values for this concentration seen in Fig. 5.
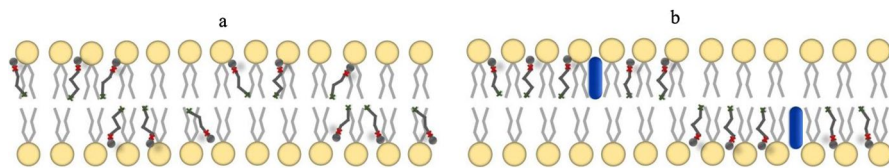
Fig. 7 Schematic presentation of clustering of stearic acids in POPC bilayer without (**a**) and with (**b**) Chalc (depicted in blue). Spin labels in 5-DSA are depicted as red crosses, and as green ones in 16-DSA. Without peptides (**a**), the clusters are divided into small sub-clusters, alternatively located in two opposing leaflets; the 5-DSA local concentration is effectively reduced because of mutual repulsing of the polar heads and inter-leaflet separation. With peptide (**b**), the sub-clusters are assembled around the peptide, becoming larger and mutually separated; see text for other details

4 Discussion

The Chalc secondary structure in POPC membranes was found to be an α-helix [30], with the full length of ~2.16 nm that is not enough to span the hydrophobic core of the POPC membrane (2.8–3.2 nm) [60]. According to the ESEEM data shown in Fig. 3, Chalc-SL is located slightly above the 5-th carbon position (closer to the membrane surface) of the embedded stearic acid. This implies that Chalc molecules are buried in the membrane interior. The α-helix diameter is around 0.5 nm [61]; taking into account also the peptide side groups (Trp, Ala, Val, Gln, Ser, Leu), the peptide outer diameter of Chalc could be estimated as ~1 nm.

The local DSA concentrations without Chalc exceed those for a uniform distribution of free fatty acids (see Fig. 5), which is in the agreement with previous results on spin-labeled stearic acids obtained using ESE decays [29] and from DEER data [38]. This unambiguously indicates clustering of DSA molecules. The twofold excess of the local concentration over the average concentration found here can be explained by alternative clustering in two opposite leaflets—see insert to Fig. 5. This type of clustering can be called a "chess box" model. The reason for such alternative clustering may be the effect of DSA molecules assembled in one lipid leaflet on the opposite lipid leaflet.

The data presented in Figs. 4 and 6 show that the presence of Chalc directly influences the DSA lateral distribution. In our previous work [38], it was found that (without Chalc) the local concentration of 5-DSA is lower than that of 16-DSA (in POPC membranes only above 1 mol% of DSA—see Fig. 5). This effect was explained [38] by mutual repulsion of the polar heads and inter-leaflet separation of spin labels, which results in increase of the distances between spin labels in 5-DSA—see schematic presentation in Fig. 7a. When Chalc is added to the lipid bilayer, data in Fig. 6 show that the C_{local} values for 5-DSA are increasing with the increase of Chalc, while those for 16-DSA are decreasing, tending to their equality. This equalization may be interpreted as reorganization of the DSA sub-clusters, in the way shown schematically in Fig. 7b. It is assumed here that DSA molecules are assembled around the Chalc, so the sub-clusters in presence of the peptides become somewhat larger and separated from each other. Due to the attraction to Chalc molecules, the mutual repulsion of the polar heads of DSA molecules in these

Chalc-DSA clusters may become less important so the local concentration of spin labels in 5-DSA becomes higher. On the other hand, due to cluster separation, the local concentration of spin labels in 16-DSA becomes lower.

For 5-DSA at the concentration of 1 mol%, the C_{local} increase this P/L increase is not observed (see Fig. 6). This can be readily explained by the equality of the apparent C_{local} values for 5-DSA and 16-DSA in the absence of peptide that is seen in Fig. 5; this equality implies that the alternative DSA clustering in two opposing leaflets does not influence the C_{local} values for this DSA concentration.

A possible mechanism of DSA attraction to the peptide molecules could be the modulation of the lipid acyl chains arrangement, which is accompanied by formation of local defects [62]. The more flexible and mobile DSA molecules adopt local voids and packing defects, thus altering the lipid conformations and relative disposition. Probably, the less bulky polar head and the single chain of free fatty acids make it more suitable for this compensation, and in this case the peptide works as its attractor [29]. This mechanism probably may select lipids—by attracting those of more flexible structures (e.g., possessing lesser number of double bonds).

The most intriguing point is that the peptide influence found in this work takes place at the extremely small peptide concentrations: the effect is seen already at 0.01 mol% (the peptide/lipid ratio P/L = 1/10,000). Note that for the similar medium-length peptide tylopeptin B structural changes in FFA clustering were observed also at low peptide concentration, ~ 0.1 mol% (P/L ~ 1/1000) [63], which however is not as small as in this work. For explanation of the found effect further investigation is needed.

Another point which needs clarification is some tendency to periodicity seen in Fig. 6 for both 5-DSA and 16-DSA. Indeed, for 2 mol% of 5-DSA one can see local minima occurring near P/L ratios of 0.03, 0.12 and 0.4 mol%. The existence of these minima certainly is above the experimental uncertainty achieved in this experiment. Note in this respect that for 1 mol% of 5-DSA data in Fig. 6 within the experimental uncertainty are nearly constant.

Note that neutron scattering experiments demonstrated that peptides of low concentrations of 0.5 or 1 mol% may disrupt a lateral inhomogeneity [22] and reduce the lipid lateral motion in the fluid phase [19]. These results were claimed to provide insights into how a short peptide kills bacteria at low concentrations without forming pores or destroying membranes.

5 Conclusions

From our EPR analysis on the medium-length peptide Chalc in lipid bilayers, we conclude that (1) the peptide is localized in the membrane interior, (2) it is not prone to specific oligomerization, and (3) starting from ultralow concentrations (~ 0.01 mol%), it induces the lateral rearrangement of free fatty acids embedded into the bilayer.

In the absence of Chalc, the local concentration of 5-DSA in the POPC bilayer is lower than that of 16-DSA. This behavior can be attributed to alternative DSA sub-clustering in the two opposing leaflets. In the presence of Chalc the local

concentration of 5-DSA increases, while that of 16-DSA decreases, thus tending toward the equalization of these two effective concentrations. This result may be interpreted assuming that the sub-clusters assemble around the peptides, becoming larger and mutually separated.

Declarations

Conflict of interest The authors declare that they have no conflict of interest.

References

1. C.L. Ventola, Pharm. Ther. **40**, 277 (2015)
2. C.L. Ventola, Pharm. Ther. **40**, 344 (2015)
3. M.D. Seo, H.S. Won, J.H. Kim, T.B. Mishig-Ochir, J. Le, Molecules **17**, 2276 (2012)
4. M. Rima, M. Rima, Z. Fajloun, J.M. Sabatier, B. Bechinger, T. Naas, Antibiotics **10**, 1095 (2021)
5. A.A. Bahar, D. Ren, Pharmaceuticals **6**, 1543 (2013)
6. M. Zasloff, Nature **415**, 389 (2002)
7. T. Neuhof, A. Berg, H. Besl, T. Schwecke, R. Dieckmann, H. von Doehren, Chem. Biodiv. **4**, 1103 (2007)
8. P.G. Lima, J.T.A. Oliveira, J.L. Amaral, C.D.T. Freitas, P.F.N. Souza, Life Sci. **278**, 119647 (2021)
9. E. Randal, Future Microbiol. **6**, 635 (2011)
10. W.L. Zhu, Y.M. Song, Y. Park, K.H. Park, S.T. Yang, J.I. Kim, I.S. Park, K.S. Hahm, S.Y. Shin, Biochim. Biophys. Acta-Biomembr **1768**, 1506 (2007)
11. M. Gobbo, M. Benincasa, G. Bertoloni, B. Biondi, R. Dosselli, E. Papini, E. Reddi, R. Rochhi, R. Tavano, R. Gennaro, J. Med. Chem. **52**, 5197 (2009)
12. M. De Zotti, B. Biondi, Y. Park, K.S. Hahm, M. Crisma, C. Toniolo, F. Formaggio, Amino Acids **43**, 1761 (2012)
13. A.J. Krauson, O.M. Hall, T. Fuselier, C.G. Starr, W.B. Kauffman, W.C. Wimley, J. Am. Chem. Soc. **137**, 16144 (2015)
14. F.G. Avci, B.S. Akbulut, E. Ozkirimli, Biomolecules **8**, 77 (2018)
15. M.F. Brown, Biochem. **51**, 9782 (2012)
16. D. Marsch, Biochim. Biophys. Acta Biomembr **1778**, 1545 (2008)
17. V.K. Sharma, E. Mamontov, M. Tyagi, S. Qian, D.K. Rai, V.S.K. Urban, J. Phys. Chem. Lett. **7**, 2394 (2016)
18. J.B. Mitra, V.K. Sharma, A. Mukherjee, V.G. Sakai, A. Dash, M. Kumar, Langmuir **36**, 397 (2019)
19. V.K. Sharma, S. Qian, Langmuir **35**, 4152 (2019)
20. R.M. Epand, S. Rotem, A. Mor, B. Berno, R.F. Epand, J. Am. Chem. Soc. **130**, 14346 (2008)
21. P. Wadhwani, R.F. Epand, N. Heidenreich, J. Bürck, A.S. Ulrich, R.M. Epand, Biophys. J. **103**, 265 (2012)
22. S. Qian, D. Rai, W.T. Heller, J. Phys. Chem. B **118**, 11200 (2014)
23. K. Hammond, M.G. Ryadnov, B.W. Hoogenboom, Biochim. Biophys. Acta Biomembr **1863**, 183447 (2021)
24. S.J. Archer, J.F. Ellena, D.S. Cafiso, Biophys. J. **60**, 389 (1991)
25. J. Pan, S. Tristram-Nagle, J.F. Nagle, J. Membr. Biol. **231**, 11 (2009)
26. R. Seyfi, F.A. Kahaki, T. Ebrahimi, S. Montazersaheb, S. Eyvazi, V. Babaeipour, V. Tarhriz, Int. J. Peptide Res. Ther. **26**, 1451 (2020)
27. V. Teixeira, M.J. Feio, M. Bastos, Progr. Lipid Res. **51**, 149 (2012)

28. E.F. Afanasyeva, V.N. Syryamina, S.A. Dzuba, J. Chem. Phys. **146**, 011103 (2017)
29. E.F. Afanasyeva, V.N. Syryamina, M. De Zotti, F. Formaggio, C. Toniolo, S.A. Dzuba, Biochim. Biophys. Acta Biomembr **1862**, 524 (2019)
30. B. Biondi, C. Peggion, M. De Zotti, C. Pignaffo, A. Dalzini, M. Bortolus, S. Oancea, G. Hilma, A. Bortolotti, L. Stella, J.Z. Pedersen, V.N. Syryamina, Y.D. Tsvetkov, S.A. Dzuba, C. Toniolo, F. Formaggio, Peptide Sci. **110**, e23083 (2018)
31. V.N. Syryamina, E.F. Afanasyeva, S.A. Dzuba, F. Formaggio, M. De Zotti, Biochim. Biophys. Acta Biomembr. **1864**, 183978 (2022)
32. K. Fa, H. Liu, H. Gong, L. Zhang, M. Liao, X. Hu, D. Ciumac, P. Li, J. Webster, J. Petkov, R.K. Thomas, J.R. Lu, Langmuir **38**, 6623 (2022)
33. S.S. Funari, F. Barceló, P.V. Escribá, J. Lipid Res. **44**, 567 (2003)
34. C.C. De Carvalho, M.J. Caramujo, Molecules **23**, 2583 (2018)
35. A.P. Desbois, V.J. Smith, Appl. Microbiol. Biotechnol. **85**, 1629 (2010)
36. R.F. Epand, P.B. Savage, R.M. Epand, Biochim. Biophys. Acta Biomembr. **1768**, 2500 (2007)
37. C. Sohlenkamp, O. Geiger, FEMS Microbiol. Rev. **40**, 133 (2016)
38. A.S. Smorygina, E.A. Golysheva, S.A. Dzuba, Langmuir **37**, 13909 (2021)
39. A.D. Milov, K.M. Salikhov, M.D. Shirov, Fiz. Tverd. Tela **23**, 975 (1981)
40. A.D. Milov, A.G. Maryasov, Yu.D. Tsvetkov, Appl. Magn. Reson. **15**, 107 (1998)
41. G. Jeschke, G. Panek, A. Godt, A. Bender, H. Paulsen, Appl. Magn. Reson. **26**, 223 (2004)
42. G. Jeschke, Biomolecules **12**, 1369 (2022)
43. K.M. Salikhov, I.T. Khairuzhdinov, R.B. Zaripov, Appl. Magn. Reson. **45**, 573 (2014)
44. D.A. Erilov, R. Bartucci, R. Guzzi, A.A. Shubin, A.G. Maryasov, D. Marsh, S.A. Dzuba, L. Sportelli, J. Phys. Chem. B **109**, 12003 (2005)
45. E.S. Salnikov, D.A. Erilov, A.D. Milov, Yu.D. Tsvetkov, C. Peggion, F. Formaggio, C. Toniolo, J. Raap, S.A. Dzuba, Biophys. J. **91**, 1532 (2006)
46. A.D. Milov, R.I. Samoilova, A.A. Shubin, Y.A. Grishin, S.A. Dzuba, Appl. Magn. Reson. **35**, 73 (2008)
47. S.A. Dzuba, D. Marsh, ESEEM of spin labels to study intermolecular interactions, molecular assembly and conformation. in *A Specialist Periodic Report, Electron Paramagnetic Resonance*, vol. 24, ed. by C. Gilbert, V. Chechik, D.M. Murphy (RSC Publishing, 2015), pp. 102–121
48. G. Pabst, S. Danner, R. Podgornik, J. Katsaras, Langmuir **23**, 11705 (2007)
49. A.D. Milov, Y.A. Grishin, S.A. Dzuba, Yu.D. Tsvetkov, Appl. Magn. Reson. **41**, 59 (2011)
50. T.I. Smirnova, A.I. Smirnov, Methods Enzym. **564**, 219 (2015)
51. D. Marsh, *Spin-Label Electron Paramagnetic Resonance Spectroscopy* (CRC Press, Boca Raton, 2020)
52. H.J. Steinhoff, N. Radzwill, W. Thevis, V. Lenz, D. Brandenburg, A. Antson, G. Dodson, A. Wollmer, Biophys. J. **73**, 3287 (1997)
53. M.E. Kardash, S.A. Dzuba, J. Phys. Chem. B **121**, 5209 (2017)
54. E.A. Golysheva, A.S. Smorygina, S.A. Dzuba, Appl. Magn. Reson. **53**, 685 (2022)
55. A.S. Kashnik, D.S. Baranov, S.A. Dzuba, Membranes **12**, 1077 (2022)
56. D. Poger, A.E. Mark, J. Chem. Theory Comput. **6**, 325 (2010)
57. N. Kučerka, M.P. Nieh, J. Katsaras, Biochim. Biophys. Acta **1808**, 2761 (2011)
58. D.S. Baranov, A.S. Smorygina, S.A. Dzuba, Molecules **27**, 4127 (2022)
59. K.B. Konov, N.P. Isaev, S.A. Dzuba, Mol. Phys. **111**, 2882 (2013)
60. L. Janosi, A.A. Gorfe, J. Chem. Theory Comput. **6**, 3267 (2010)
61. G.E. Schulz, R.H. Schirmer, *Principles of Protein Structure* (Springer Science & Business Media, Berlin, 2013)
62. B. Bechinger, J. Pept. Sci. **21**, 346 (2015)
63. V.N. Syryamina, N.E. Sannikova, M. De Zotti, M. Gobbo, F. Formaggio, S.A. Dzuba, Biochim. Biophys. Acta Biomembr. **1863**, 183585 (2021)